

## Processing and properties of Al–Li–SiC<sub>p</sub> composites

Ranjit Bauria & M.K. Surappa

To cite this article: Ranjit Bauria & M.K. Surappa (2007) Processing and properties of Al–Li–SiC<sub>p</sub> composites, Science and Technology of Advanced Materials, 8:6, 494–502, DOI: [10.1016/j.stam.2007.07.004](https://doi.org/10.1016/j.stam.2007.07.004)

To link to this article: <https://doi.org/10.1016/j.stam.2007.07.004>



© Elsevier Science Ltd



Published online: 21 Aug 2007.



Submit your article to this journal [↗](#)



Article views: 80



View related articles [↗](#)



Citing articles: 21 View citing articles [↗](#)



# Processing and properties of Al–Li–SiC<sub>p</sub> composites

Ranjit Bauri<sup>a,\*</sup>, M.K. Surappa<sup>b</sup>

<sup>a</sup>Department of Metallurgical and Materials Engineering, Indian Institute of Technology Madras, Chennai 600036, India

<sup>b</sup>Department of Materials Engineering, Indian Institute of Science, Bangalore 560012, India

Received 3 May 2007; received in revised form 20 June 2007; accepted 13 July 2007

Available online 21 August 2007

## Abstract

Al–Li–SiC<sub>p</sub> composites were fabricated by a modified version of the conventional stir casting technique. Composites containing 8, 12 and 18 vol% SiC particles (40 μm) were fabricated. Hardness, tensile and compressive strengths of the unreinforced alloy and composites were determined. Ageing kinetics and effect of ageing on properties were also investigated. Additions of SiC particles increase the hardness, 0.2% proof stress, ultimate tensile strength and elastic modulus of Al–Li–8%SiC and Al–Li–12%SiC composites. In case of the composite reinforced with 18% SiC particles, although the elastic modulus increases the 0.2% proof stress and compressive strength were only marginally higher than the unreinforced alloy and lower than those of Al–Li–8%SiC and Al–Li–12%SiC composites. Clustering of SiC particles appears to be responsible for reduced the strength of Al–Li–18%SiC composite. The fracture surface of unreinforced 8090 Al–Li alloy (8090Al) shows a dimpled structure, indicating ductile mode of failure. Fracture in composites occurs by a mixed mode, giving rise to a bimodal distribution of dimples in the fracture surface. Cleavage of SiC particles was also observed in the fracture surface of composites. Composites show higher peak hardness and lower peak ageing time compared with unreinforced 8090Al alloy. Macro- and microhardness increase significantly after peak ageing. Ageing also results in considerable improvement in strength of the unreinforced 8090Al alloy and its composites. This is attributed to formation of δ' (Al<sub>3</sub>Li) and S' (Al<sub>2</sub>CuMg) precipitates during ageing. Per cent elongation, however, decreases due to age hardening. Al–Li–12%SiC, which shows marginally lower UTS and compressive strength than the Al–Li–8%SiC composite in extruded condition, exhibits higher strength than Al–Li–8%SiC in peak-aged condition. © 2007 NIMS and Elsevier Ltd. All rights reserved.

**Keywords:** Al–Li alloy; Particle-reinforced composite; Mechanical properties

## 1. Introduction

In the recent years, usage of ceramic particle-reinforced metal matrix composites (MMCs) is steadily increasing. Aluminium matrix composites (AMCs) have gained wide acceptance in the past three decades due to their high specific strength and stiffness and superior wear resistance [1–4]. A number of processing routes has been developed for the manufacture of particle/whisker/short fibre-reinforced composites. Although these methods are capable of generating material of high microstructural quality, their widespread use is limited due to high costs associated with many of these methods. Melt stirring or the stir casting technique is currently one of the simplest and most economical fabrication routes employed to manufacture

particle-reinforced composites. However, a large number of process variables must be controlled in the melt stirring technique to achieve a high degree of microstructural integrity. Use of non-optimal parameters could lead to low-density and low-quality microstructures and this will in turn lead to poor mechanical properties.

The constant need for higher fuel efficiency in aerospace and automobile industries has led to the development of low-density Al–Li alloys. Additions of 1% Li can reduce the density by about 3%, with concomitant increase in strength and stiffness [5]. It is quite logical to think of reinforcing Al–Li alloys with ceramic particles in order to achieve further increase in strength and stiffness. Although some studies have been done on Al–Li alloy-based composites in recent years [6–9], Al–Li alloy-based composites have received relatively limited attention. This may be due to the hazards associated with Li handling during alloying. A carefully maintained atmosphere or

\*Corresponding author. Tel.: +91 44 22574778; fax: +91 44 22574752.  
E-mail address: [rbauri@iitm.ac.in](mailto:rbauri@iitm.ac.in) (R. Bauri).

vacuum is needed to prevent loss of Li and the associated fire hazard/burning at the processing temperature, and all these lead to high processing/material costs. In this study, a simple and cost-effective experimental set-up has been used by modifying the conventional stir casting technique for the fabrication of Al–Li–SiC<sub>p</sub> composites. Further, mechanical properties of SiC particle-dispersed Al–Li–SiC<sub>p</sub> composites and their age-hardening kinetics have also been studied.

## 2. Experimental procedure

### 2.1. Material selection and composite preparation

The aluminium alloy used as matrix material in the present study is an 8090 Al–Li alloy (8090Al) whose elemental composition is given in Table 1. SiC particles used as reinforcement had an average size of 40 μm. The experimental set-up used for fabricating the composites is a simple modification of the conventional melt stirring technique, which has been described in detail by Surappa and Rohatgi [10] in the early years. A schematic diagram of the casting set-up used in the present study is shown in Fig. 1. The modification comes in the form of a steel hood, which has been used as a gas cover to make an inert atmosphere in order to prevent loss of lithium. In previous studies, stirring of the melt had been done either in open air [10,11] or using a furnace with a provision for creating an inert environment [12]. This kind of environment furnace restricts direct view of the melt during melting and stirring. The simple improvisation used in this study excludes the need of using such furnaces and prevents loss of Li at the same time. The steel hood (gas cover) can be lifted or tilted to have a view of the melt. This also allows measurement of temperature of the melt conveniently by dipping a thermocouple as and when required. The steel hood can also be tilted and held at one side (on the other side an argon-carrying pipe is held as described below) to provide additional inert gas cover during stirring. The matrix alloy was melted in a stainless-steel crucible in a resistance-heated furnace. The furnace was covered with the steel hood (gas cover) and argon gas was passed through it to prevent loss of Li and any fire hazard (Fig. 1(a)). The gas cover was removed just prior to addition of SiC particles. Preheated SiC particles were added through the periphery of the vortex, which was created by stirring the melt with a mechanical impeller. As shown in Fig. 1(b) a protective atmosphere was maintained during stirring by holding an argon-carrying pipe over the melt. After the additions and thorough mixing, the melt was poured into cylindrical cast

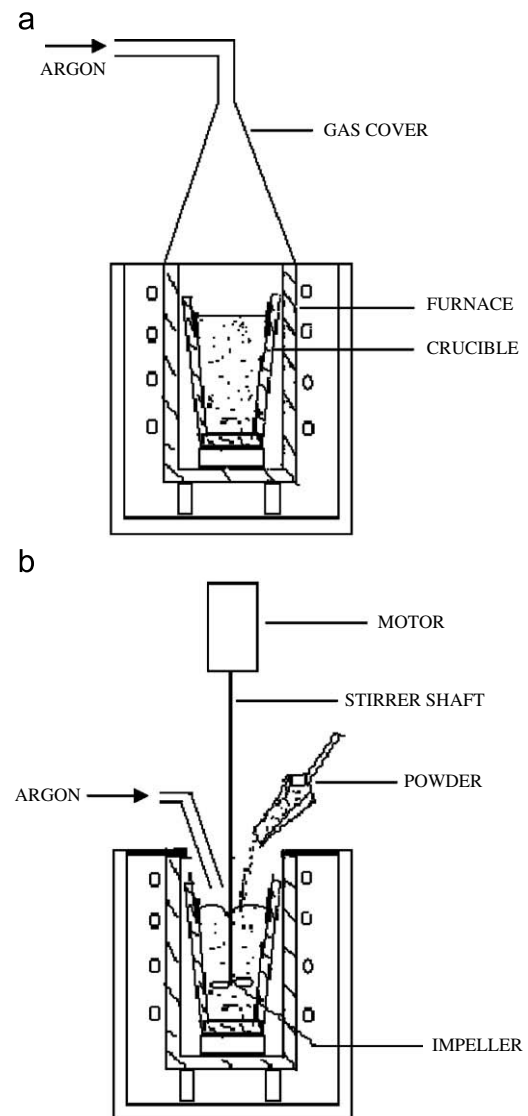


Fig. 1. Schematic diagram of the stir casting set-up used for fabricating the composites (a) before SiC<sub>p</sub> additions and (b) during the addition of particles.

iron moulds. Composites containing 8, 12 and 18 vol% SiC particles were fabricated successfully. The cast ingots were hot extruded at 540 °C in a CBJ 250 tonne extrusion press with an extrusion ratio of 30:1. Al–Li–8%SiC, Al–Li–12%SiC and Al–Li–18%SiC composites fabricated and used in this study are designated as MMC 8, MMC 12 and MMC 18, respectively, and this will be followed hereafter. Specimens for microstructural characterization and mechanical testing (hardness, tensile and compressive) were made from the extruded rod.

### 2.2. Microstructural characterization

The morphology of the SiC particles was examined by a scanning electron microscope (SEM). Sliced samples of unreinforced alloy and composites were first polished with emery paper up to 1200 grit size, followed by polishing with

Table 1  
Composition of the alloy (wt%)

Li	Cu	Mg	Zr	Fe	Si	Al
2.14	2.0	0.88	0.12	0.1	<0.03	Bal.

SiC suspension on a velvet cloth. Finally the samples were polished with 0.5  $\mu\text{m}$  diamond paste. Microstructural characterization of the polished samples was done by SEM and optical microscopy. The grain morphology of the unreinforced alloy, distribution and volume fraction of SiC particles in the composites were determined by a standard metallographic technique. The grain size was determined using Sigma scanpro image analyser.

The volume fraction of SiC was also determined by the chemical dissolution method. Samples from different portion of the extruded rod were cut and weighed in an electronic balance with an accuracy of 0.1 mg. The samples were then dissolved in dilute HCl and the solution was filtered to separate the SiC particles. The residue (SiC) was then dried by heating to a temperature of 70  $^{\circ}\text{C}$  for 45 min and the weight of the dried residue was taken. The volume fraction is calculated from the relation

$$V_p = \frac{(m_p/\rho_p)}{(m_p/\rho_p + m_m/\rho_m)}, \quad (1)$$

where  $V_p$  is the volume fraction of particles,  $m_p$  and  $m_m$  are the mass of reinforcement and matrix, respectively, and  $\rho_p$  and  $\rho_m$  are the densities of the reinforcement and the matrix alloy, respectively.

The density was determined by standard Archimedes' principle. The percent porosity was calculated from the difference between theoretical and measured densities.

### 2.3. Mechanical properties

#### 2.3.1. Micro- and macrohardness measurements

Vickers microhardness of the unreinforced alloy and composites was measured using a Dynamic Ultra Micro Hardness tester (DUH-202) at a load of 25 g in the as-cast, extruded and peak-aged conditions. Microhardness measurements were made on the matrix away from SiC particles. Brinell macrohardness was measured using an Indentec Hardness Tester. A load of 62.5 kg was used for Brinell hardness measurements.

#### 2.3.2. Tensile and compressive tests

Room-temperature tensile properties were measured using standard ASTM tensile test specimens. Tests were carried out using an Instron 8501 servo hydraulic machine at a strain rate of  $10^{-3} \text{ s}^{-1}$ . The fracture surface was observed under SEM. For compressive tests, cylindrical specimens with a diameter of 8 mm and a height of 12 mm were used. Some concentric grooves were made at both faces of the specimen to retain the lubricant. Geometries of tensile and compressive specimens are shown in Figs. 2(a) and (b), respectively. Compressive tests were carried out using a Dartec machine at room temperature with a constant strain rate of  $10^{-3} \text{ s}^{-1}$ . The elastic modulus of the alloy and its composites were determined by the sonic resonance method using an Elasto sonic instrument. Tensile and compressive tests were also done at peak-aged

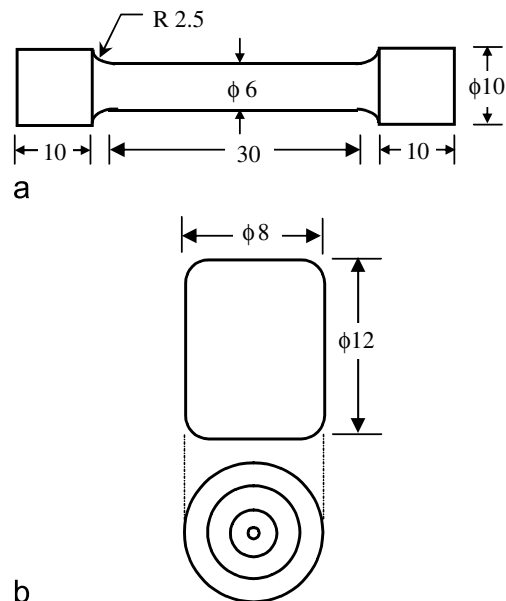


Fig. 2. Geometries of (a) tensile and (b) compressive specimen (all dimensions are in mm).

condition to assess the effect of heat treatment on mechanical properties.

### 2.4. Age hardening

Samples were heated to 530  $^{\circ}\text{C}$  in a vertical tube furnace for 1 h and then quenched in water kept at room temperature. The quenched samples were immediately transferred to an oil bath and heated to a temperature of 165  $^{\circ}\text{C}$  for ageing. Microhardness measurements were done at an interval of 1 h to determine the peak hardness and time to peak ageing. A DUH-202 microhardness tester was used to measure microhardness. A minimum of five hardness measurements were made on each sample.

## 3. Results and discussion

### 3.1. Microstructure

The SEM micrograph in Fig. 3 shows that SiC particles are irregular in shape. Optical micrographs in Figs. 4 and 5 show the grain morphology of unreinforced alloy and MMC 8, respectively, in as-cast conditions. Composites exhibit finer grain size compared with the unreinforced alloy. In particle-reinforced MMCs, particles refine the matrix grain size since dispersed particles act as nucleation sites. The average grain size of composites MMC 8, MMC 12 and MMC 18 is 36, 27 and 25  $\mu\text{m}$ , respectively, and that of the unreinforced alloy is 48  $\mu\text{m}$ . It can also be noted that as the SiC content increases, the grain size decreases. Figs. 6(a)–(c) show the distribution of SiC particles in the composites in extruded conditions. Distribution of SiC particles is fairly uniform in MMC 8; however, the other two composites having higher amounts of SiC<sub>p</sub>, i.e., MMC

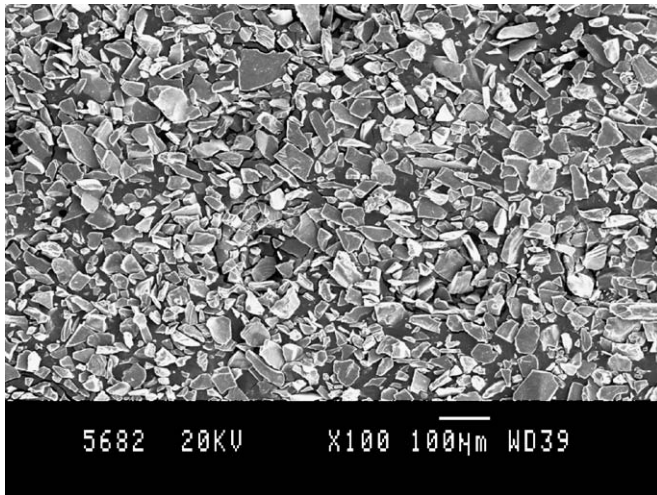


Fig. 3. SEM micrograph showing morphology of SiC particles.

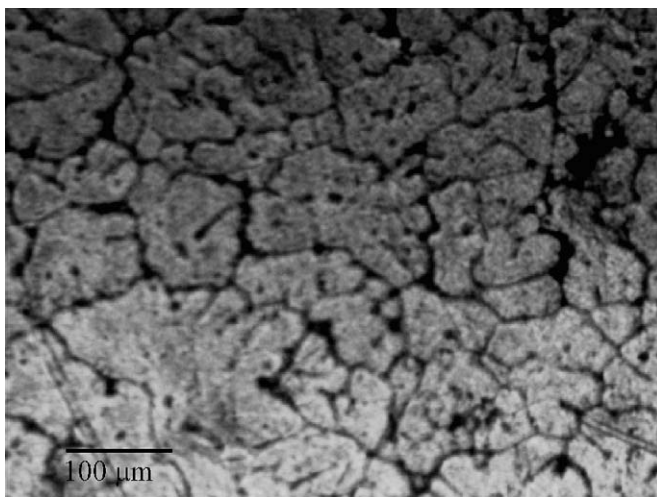


Fig. 4. Optical micrograph of the as-cast unreinforced 8090Al alloy showing grain morphology.

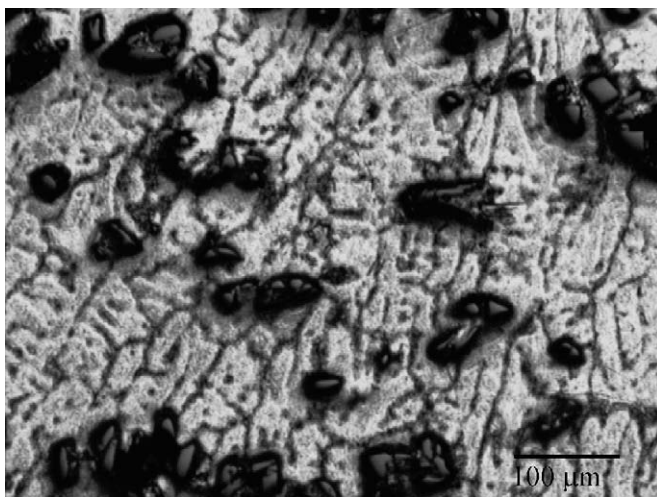


Fig. 5. Optical micrograph showing grain morphology of composite MMC 8 in the as-cast condition.

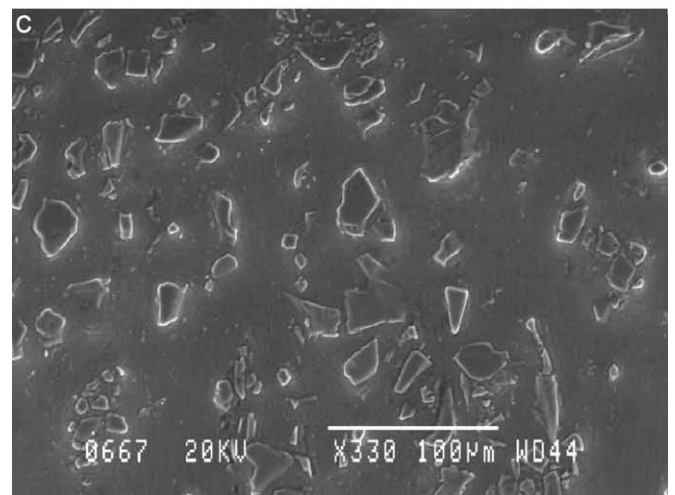
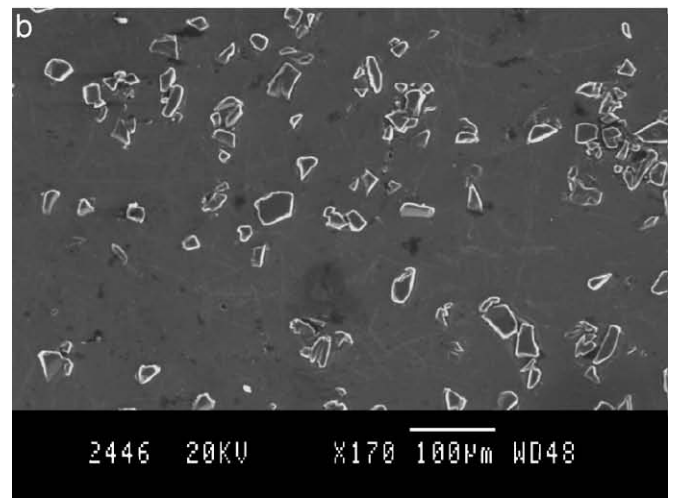
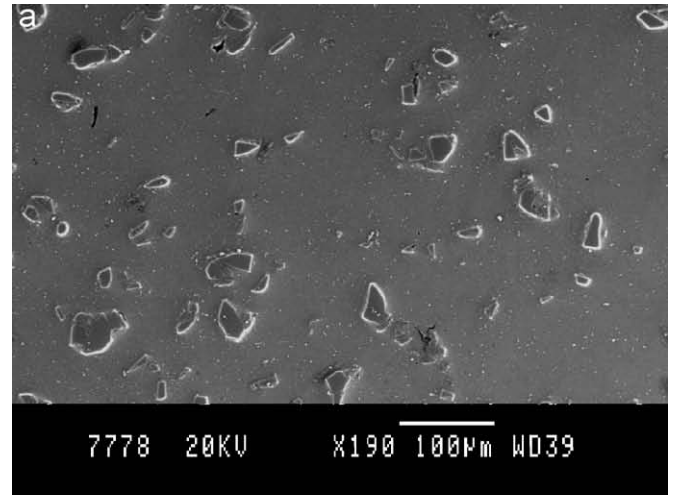


Fig. 6. SEM micrographs of the composites in extruded condition, showing distribution of SiC particles; (a) MMC 8; (b) MMC 12; and (c) MMC 18.

12 and MMC 18, show some clustering of the particles. The extent of clustering is higher in MMC 18. Fig. 7 shows a cluster of particles lying in the extrusion direction in the elongated form in this composite. The interfacial bonding between SiC particles and matrix was also observed under

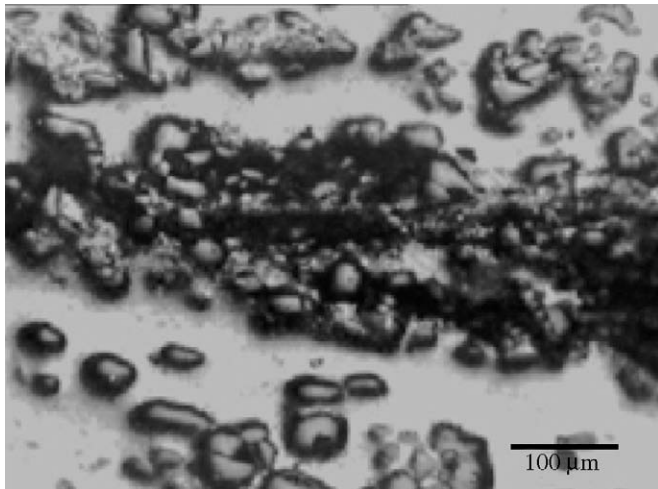


Fig. 7. Optical micrograph showing a band of  $\text{SiC}_p$  cluster elongated in the extrusion direction in the MMC 18 composite.

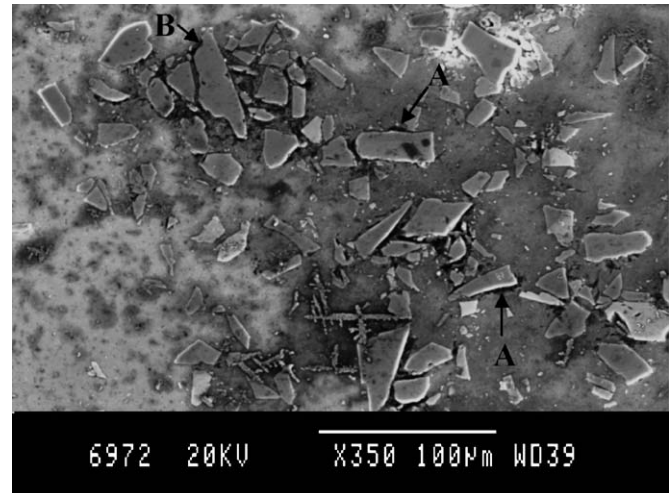


Fig. 9. SEM micrograph showing interface cracking at some local regions in MMC 18: (A) crack at an individual particle and (B) crack in a cluster.

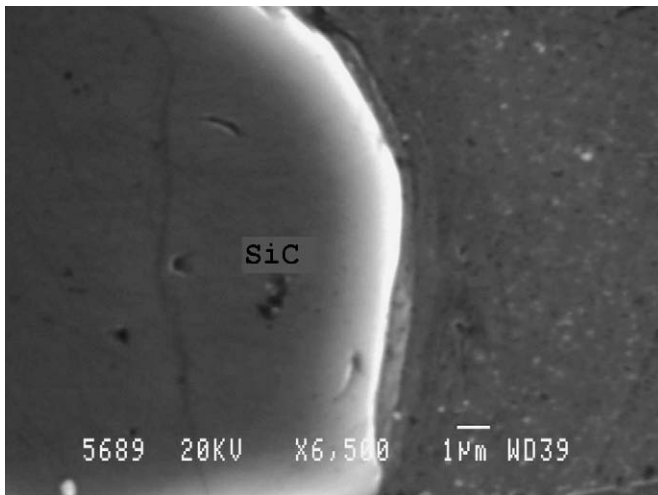


Fig. 8. SEM micrograph showing particle–matrix interface in the MMC 8 composite.

SEM. The bonding is good and there is no sign of any interfacial reaction. The SEM micrograph in Fig. 8 shows the particle–matrix interface in the MMC 8 composite. However, some cracking at the interface was found at some local regions in MMC 18 (Fig. 9). This is due to the high thermal stresses generated at the interface during cooling as a result of the large difference in coefficient of thermal expansion between the matrix and the particles. Although similar thermal mismatch exists in MMC 8 and MMC 12, this kind of interfacial disintegration was not observed in these composites. This can be attributed to the higher volume fraction of SiC in MMC 18. The higher volume fraction of particles is expected to generate greater thermal stresses. Moreover, as described above, MMC 18 contains some cluster of SiC particles. These clusters can generate high thermal stresses and lead to cracking at the interface (site B in Fig. 9).

Table 2  
Density and porosity of the 8090Al alloy and its composites

Material	As cast		Extruded	
	Density (kg/m <sup>3</sup> )	Porosity (%)	Density (kg/m <sup>3</sup> )	Porosity (%)
8090Al alloy	2490	2.07	2540	0.12
MMC 8	2510	3.42	2580	0.60
MMC 12	2450	6.40	2600	0.90
MMC 18	2290	13.70	2620	1.35

### 3.2. Density and porosity

Table 2 shows the results of density and porosity measurements. Although almost 100% densification is achieved in the alloy and MMC 8 composite, some amount of porosity is present in MMC 12 and MMC 18 composites in the extruded condition. This porosity is mainly due to dissolved gases ( $\text{H}_2$ ). Higher the amount of  $\text{SiC}_p$  reinforcement, higher the amount of gas porosity.

### 3.3. Mechanical properties

#### 3.3.1. Micro- and macrohardness

Tables 3 and 4 show macro- and microhardness, respectively, of the unreinforced alloy and composites in the as-cast and extruded conditions. Composite MMC 8 shows higher macrohardness than the unreinforced alloy in both as-cast and extruded conditions. On the other hand, composites MMC 12 and MMC 18 show lower hardness than the alloy in the as-cast condition. This is due to higher amount of porosity present in these two composites in the as-cast condition (Table 2). However, after extrusion the pores are closed and as a result these two composites

exhibit higher hardness than the unreinforced alloy in the extruded condition. The microhardness of all the composites studied are higher than the unreinforced alloy in both as-cast and extruded conditions. The matrix of composites contains higher dislocation density due to mismatch in thermal expansion coefficient between the matrix and the reinforcement. This leads to higher hardness in the composites. As discussed above, the presence of SiC particles refines the grain size. Finer grain size in composites also leads to higher hardness.

Table 3  
Macrohardness (BHN) of the 8090Al alloy and its composites in the as-cast, extruded and peak-aged conditions

Material	As cast	Extruded	Peak aged
8090Al alloy	98.7	84	107
MMC 8	104	89	110
MMC 12	96.7	108	117
MMC 18	73	111	120

Table 4  
Microhardness (VHN) values in as-cast, extruded and peak-aged conditions

Material	As cast	Extruded	Peak aged
8090Al alloy	106	93	166
MMC 8	109	103	172
MMC 12	117	107	174
MMC 18	122	110	178

Table 5  
Tensile properties of the unreinforced 8090Al alloy and its composites

Material	As extruded			Peak aged		
	0.2% Proof stress (MPa)	UTS (MPa)	$e_f$ (%)	0.2% Proof stress (MPa)	UTS (MPa)	$e_f$ (%)
8090Al alloy	200	303	12.2	287	342.8	8.5
MMC 8	319	368	10.7	385	421.7	9.5
MMC 12	308	326	9.8	367	423.9	8.7
MMC 18	223	249	8.2	258	267.0	7.9

Table 6  
Compressive properties of the unreinforced 8090Al alloy and its composites

Material	As extruded			Peak aged		
	0.2% Proof stress (MPa)	Compressive strength (MPa)	$e_f$ (%)	0.2% Proof stress (MPa)	Compressive strength (MPa)	$e_f$ (%)
8090Al	211.76	517	34.0	285.29	551	23.1
MMC 8	305.55	633	27.2	388.88	729	26.5
MMC 12	304.70	618	26.0	381.38	740	25.1
MMC 18	227.60	532	25.2	250.00	623	24.5

### 3.3.2. Tensile and compressive properties

Table 5 shows the tensile properties of 8090Al alloy and its composites. It can be seen from Table 5 that the composites containing up to 12 vol% SiC exhibit higher 0.2% proof stress and ultimate tensile strength (UTS) compared with the unreinforced alloy. However, it can be observed that increase in 0.2% proof stress in MMC 18 is very marginal. Further, 0.2% proof stress and UTS of MMC 18 composite is lower than those of MMC 8 and MMC 12 and its UTS is lower than that of unreinforced alloy in the extruded condition. MMC 12 exhibits a significant increase in 0.2% proof stress and UTS over that of the unreinforced alloy but shows marginally lower UTS than MMC 8.

Table 6 shows the compressive properties of the 8090Al alloy and its composites. Although 0.2% proof stress and compressive strength of MMC 18 are marginally higher than the unreinforced alloy, these are lower compared with MMC 8 and MMC 12.

MMC 8 shows highest strength in the as-extruded condition. This can be explained in the light of integrity of microstructure vis-a-vis particle clustering and porosity. The interface between the reinforcement and matrix plays a determining role on mechanical properties of composites [13,14]. Main strengthening in composites comes from effective transfer of load from the matrix to the particle via the interface [15–17]. Therefore, in order to realize the strengthening effect of the reinforcement, the interfacial bonding between the particle and matrix must be strong. As described earlier, in the MMC 18 composite some cracks were found in some local regions at the interface between the matrix and particle due to the high thermal stresses generated at the interface during cooling as a result

of the large difference in coefficient of thermal expansion between the matrix and the particles. This may lead to decohesion of particles at the particle–matrix interface and early failure. Also, defects, which include  $\text{SiC}_p$  clusters and associated pores, contribute to observed weakening in this composite. As can be seen from Table 2 some porosity is still present even after extrusion and particles are found in association with pores (Fig. 10). These particles are not well bonded to the matrix and do not contribute to the strengthening of the composite. These loosely held particles are easily debonded during the loading process and lead to early fracture of the composite. Further, as discussed above, the MMC 18 composite exhibits a heterogeneous microstructure, with bands of  $\text{SiC}$  particle clusters lying along the extrusion direction (Fig. 7). These clusters are also the potential sites for damage accumulation. Previous studies have shown that deformation begins in regions containing clusters of particles [18,19]. As clusters are stiffer, after satisfying deformation compatibility, the stress would be distributed in such a way that the clusters would bear more load than the rest of the matrix. Secondly, since the local volume fraction is higher within the clusters, for the same amount of deformation the clusters must activate more slip systems in the matrix to accommodate the same amount of deformation [18]. This leads to fracture of clusters at an early stage. MMC 18 contains about 3% clusters. Thus, the clustering in MMC 18 also leads to decreases in ultimate tensile and compressive strengths. MMC 8 on the other hand exhibits a fairly uniform distribution of  $\text{SiC}$  particles, and the integrity of interfacial bonding between particles and matrix is also very good. Hence, MMC 8 exhibits superior properties. Although MMC 12 exhibits substantial improvement in strength over that of the unreinforced alloy, it has lower ultimate strength compared with MMC 8. This could also be due to the small amount of  $\text{SiC}_p$  clusters present in this composite. Table 7 shows the modulus values of the unreinforced alloy and the composites measured by the

Table 7  
Elastic modulus of the unreinforced 8090Al alloy and its composites

Material	Elastic modulus (GPa)
8090Al alloy	79
MMC 8	87
MMC 12	90
MMC 18	95

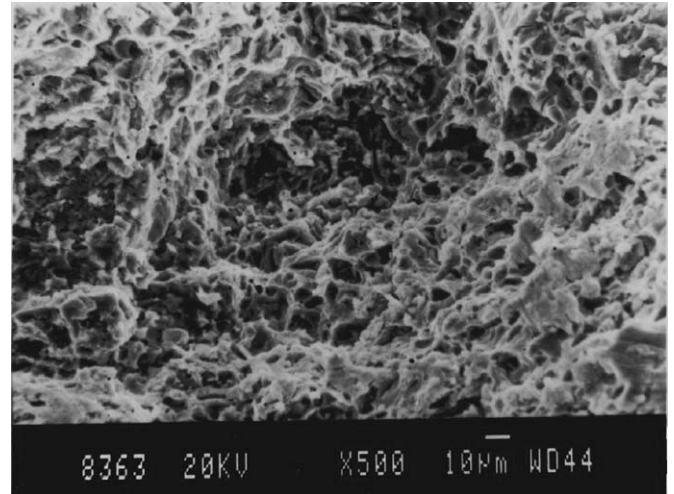


Fig. 11. SEM micrograph of fracture surface of the unreinforced 8090Al alloy.

sonic resonance method. Composites show higher elastic modulus compared with the unreinforced alloy.

SEM micrograph of fracture surface of the unreinforced alloy (Fig. 11) shows a network of dimples indicating ductile fracture mode. Fracture in MMCs occurs by mixed mode, giving rise to a bimodal distribution of dimples in the fracture surface, which is shown in Fig. 12 for MMC 8. Larger dimples are associated with  $\text{SiC}$  particles, whereas smaller dimples are associated with ductile failure of the matrix. Cleavage of  $\text{SiC}$  particles is also observed. The higher magnification SEM fractograph in Fig. 13 shows such a cleaved particle in the MMC 8 composite. It can be observed from this micrograph that there is no decohesion between the particle and the matrix, suggesting a strong interfacial bonding between particle and matrix in this composite. On the other hand, the SEM micrograph of fracture surface of the MMC 18 composite (Fig. 14) shows particle debonding. This kind of decohesion of particles from the matrix under tensile loading appears to be responsible for the degradation of mechanical properties in the MMC 18 composite.

### 3.4. Ageing behaviour

Fig. 15 shows the ageing curves (plots of hardness vs. ageing time) of 8090Al alloy and its composites aged at  $165^\circ\text{C}$ . Hardness increases with ageing time, achieving peak value and thereafter decreases. The matrix alloy

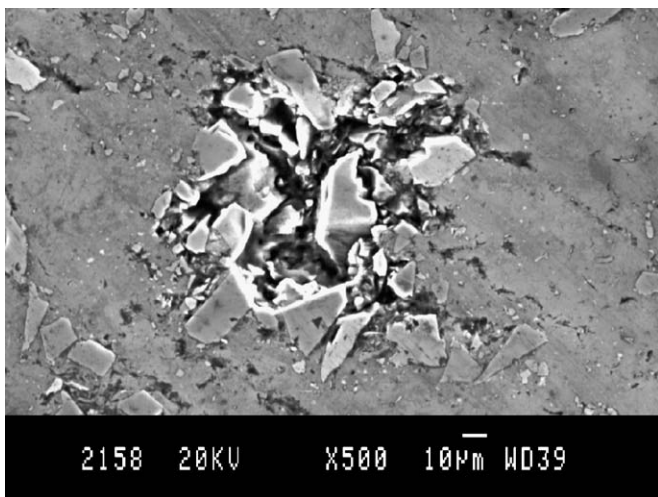


Fig. 10. SEM micrograph showing cluster of  $\text{SiC}_p$  in association with pore in MMC 18.

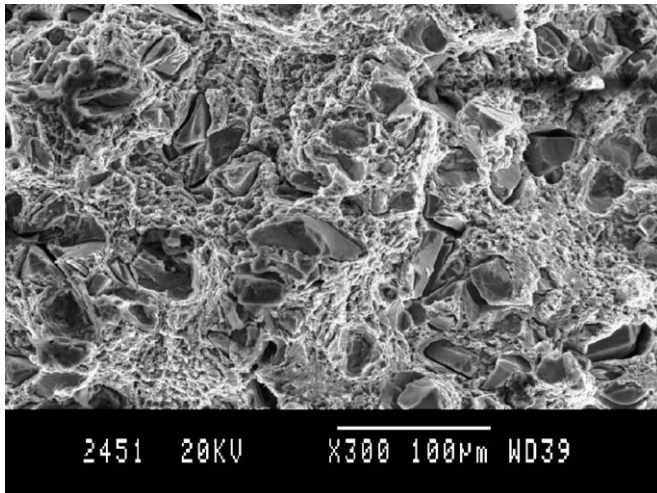


Fig. 12. SEM micrograph taken from MMC 8 showing typical fracture surface of composite.

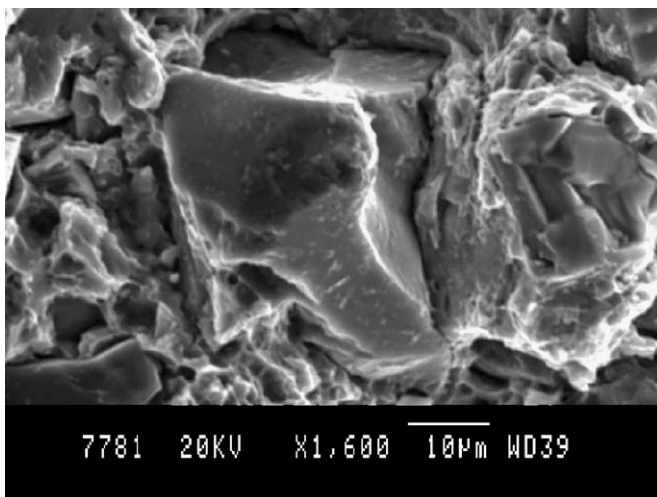


Fig. 13. Fracture surface showing a cleaved particle and strong interfacial bonding in MMC 8.

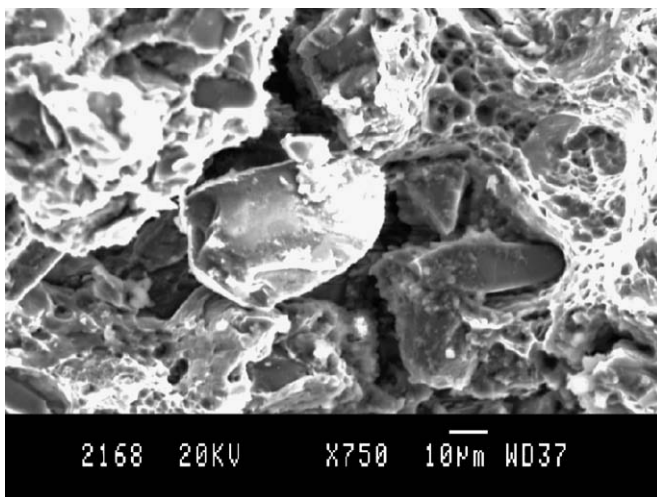


Fig. 14. SEM micrograph showing a debonded particle on the fracture surface of MMC 18.

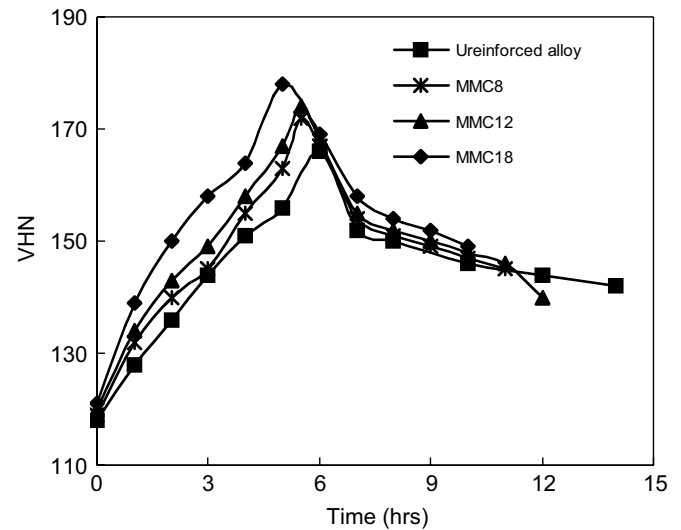


Fig. 15. Ageing curves of the unreinforced 8090Al alloy and its composites aged at 165°C.

contains Li, Cu and Mg, which form  $\delta'$  ( $\text{Al}_3\text{Li}$ ) and  $S'$  ( $\text{Al}_2\text{CuMg}$ ) precipitates during ageing, causing an increase in hardness. After the peak ageing time larger precipitates grow at the expense of smaller ones, resulting in a decrease in hardness. It can be observed that peak hardness is higher and peak ageing time is lower in composites compared with the unreinforced alloy. The peak hardness in MMC 8, MMC 12 and MMC 18 is 172, 174 and 178, respectively, compared with 166 in the unreinforced alloy. The peak ageing times in these composites are 5.5, 5.5 and 5 h, respectively, compared with 6 h for the unreinforced alloy. The main strengthening precipitates in the matrix alloy are  $\delta'$  and  $S'$ .  $S'$  precipitates nucleate heterogeneously on discontinuities like dislocations [20]. Composites contain higher dislocation density near the particle–matrix interface due to the large difference in thermal expansion coefficient between the matrix and reinforcement. Therefore, a large number of precipitates is present in composites, giving rise to higher peak hardness and shorter peak ageing time.

### 3.5. Effect of ageing on mechanical properties

Both macro- and microhardness increase significantly after peak ageing (Tables 3 and 4). Tables 5 and 6 also show the tensile and compressive properties in peak-aged condition. It can be seen that there is a considerable improvement in strength of the alloy and composites after peak ageing, due to the formation of hardening precipitates. As discussed above in the previous section, the matrix alloy contains Li, Cu and Mg, which form  $\delta'$  ( $\text{Al}_3\text{Li}$ ) and  $S'$  ( $\text{Al}_2\text{CuMg}$ ) precipitates during ageing. These precipitates give rise to hardening and increase the strength and hardness. Per cent elongation, however, reduces due to ageing. It can also be observed from Tables 5 and 6 that MMC 12 shows higher ultimate tensile and compressive

strength than MMC 8 in peak-aged condition. The strengthening effect of precipitation seems to outweigh the detrimental effect of SiC<sub>p</sub> clusters.

#### 4. Conclusions

Al–Li–SiC<sub>p</sub> composites are fabricated by a simple and cost-effective stir casting technique. Composites show higher 0.2% proof stress and higher modulus compared with the unreinforced alloy. Al–Li–8%SiC composite exhibits superior mechanical properties compared with the unreinforced alloy and the other two composites (Al–Li–12%SiC and Al–Li–18%SiC). This is due to homogeneous distribution of particles and good interfacial bonding in Al–Li–8%SiC composite. However, Al–Li–12%SiC composite shows higher ultimate tensile and compressive strength compared with Al–Li–8%SiC in peak-aged condition. All the composites exhibit higher peak hardness and accelerated ageing compared with the unreinforced alloy.

#### Acknowledgements

Thanks are due to Dr. A.K. Gokhle of the Defence Metallurgical Research Laboratory, India, for providing the Al–Li alloy used in this investigation. Thanks are also due to the Chairman, Department of Materials Engineering, Indian Institute of Science, Bangalore, India, for providing all the facilities for carrying out this study.

#### References

- [1] M.K. Surappa, P.K. Rohatgi, *J. Mater. Sci.* 16 (1981) 983.
- [2] M. Vasudevan, M.K. Surappa, in: P. Ramakrishnan (Ed.), *Proceedings of the International Conference on Advanced Composite Materials*, Oxford & IBH Publishing Co. Ltd., 1990, 265pp.
- [3] R.J. Arsenault, L. Wang, C.R. Feng, *Acta Metall. Mater.* 39 (1991) 47.
- [4] B.N. Pramila Bai, B.S. Ramashesh, M.K. Surappa, *Wear* 157 (1992) 295.
- [5] K.K. Sankaran, N.J. Grant, *Mater. Sci. Eng.* 44 (1980) 213.
- [6] P. Poza, J. Llorca, *Metall. Mater. Trans.* 30A (1999) 845.
- [7] R. Bauri, M.K. Surappa, *Metall. Mater. Trans.* 36A (3) (2005) 667.
- [8] R. Bauri, M.K. Surappa, *Mater. Sci. Eng. A* 393 (2005) 22.
- [9] R. Bauri, V. Pancholi, I. Samajdar, M.K. Surappa, *Sci. Technol. Adv. Mater.* 6 (2005) 933.
- [10] M.K. Surappa, P.K. Rohatgi, *Met. Technol.* 5 (1978) 358.
- [11] R. Mitra, V.S. Chalapathi Rao, R. Maiti, M. Chakraborty, *Mater. Sci. Eng. A* 379 (2004) 391.
- [12] V. Laurent, P. Jarry, G. Regazzoni, D. Apelian, *J. Mater. Sci.* 27 (1992) 4447.
- [13] P.K. Rohatgi, S. Ray, R. Asthana, C.S. Narendranath, *Mater. Sci. Eng. A* 162 (1993) 163.
- [14] M.Y. Gu, Z.A. WU, Y.P. Jin, M. Kocak, *J. Mater. Sci.* 35 (2000) 2499.
- [15] A. Kelly, *Strong Solids*, second ed, Clarendon, Oxford, 1972.
- [16] M.R. Piggot, *Load-bearing Fibre Composites*, Pergamon, Oxford, 1980.
- [17] B.D. Agarwal, L.J. Broutman, *Analysis and Performance of Fiber Composites*, Wiley, New York, 1980.
- [18] R.J. Arsenault, N. Shi, C.R. Feng, L. Wang, *Mater. Sci. Eng. A* 131 (1991) 55.
- [19] S.-J. Hong, H.-M. Kim, D. Huh, C. Suryanarayana, B. Sun Chun, *Mater. Sci. Eng. A* 347 (2003) 198.
- [20] R.U. Vaidya, Z.R. Xu, X. Li, K.K. Chawla, A. Zurek, *J. Mater. Sci.* 29 (1994) 2944.